Applications of nonlinear control to a whole-brain network of FHN oscillators

Teresa Chouzouris, Nicolas Roth, and Klaus Obermayer
Institut für Softwaretechnik und Theoretische Informatik,
Technische Universität Berlin
Marchstraße 23, 10587 Berlin, Germany
(Dated: February 24, 2020)

An article usually includes an abstract, a concise summary of the work covered at length in the main body of the article. **max 500 words, 5% of absolute word count**, detailed info at: `https://journals.aps.org/pre/authors`.

Usage: Secondary publications and information retrieval purposes.

Structure: You may use the `description` environment to structure your abstract; use the optional argument of the `\item` command to give the category of each item.

I. INTRODUCTION

. . . I wrote that a long time ago:

Computational models of cortical networks are a promising tool to understand the relationship between anatomical and functional organization of the brain. It is important to have a thorough understanding of the system's dynamical landscape and the influence that each parameter has on it. While it became a standard procedure to restrict the dynamics by fitting its parameters to resting state fMRI data, there is no study of what dynamical states are supported in the first place, and how the differ between subjects. Here we show what kind of dynamic states can be supported by the collective dynamics of FitzHugh-Nagumo oscillators on a network topology based on the human connectome. The experimental data is obtained from 12 young, healthy adults (26-30yrs, all male) via diffusion tensor imaging and probabilistic fibre tracking.

For abstract or intro: In this study we implement a network model simulating spatiotemporal activity in the brain and using methods from nonlinear control theory we optimize the stimulation effects. The network's topology is defined by empirical structural connectivity data. The neuronal activity of each brain region is simulated by the phenomenological FitzHugh-Nagumo model. We systematically explore the network's state space for varying parameters, and characterize the emerging dynamical network states. Next, we add external control to the nodes. By defining a minimization problem for the above system, we analyse the external stimuli that optimize the input energy. We tune the number of controlled brain regions by applying sparse optimal control. . . .

II. NETWORK MODEL

$$\begin{aligned}\frac{d}{dt}x_{1k}(t) &= h_1(\mathbf{x}_k(t)) + \sigma\sum_{i=1}^{N}\mathbf{A}_{ki}x_{1i}(t) + \eta\xi_k(t) + u_k(t)\\ \frac{d}{dt}x_{2k}(t) &= h_2(\mathbf{x}_k(t))\end{aligned} \tag{1}$$

$$\begin{aligned}\frac{d}{dt}\mathbf{x}(t) = \mathbf{h}(\mathbf{x}(t)) &+ \sigma(\mathbf{A}\otimes\mathbf{G})\mathbf{x}(t)\\ &+(\mathbf{B}\otimes\mathbf{K})\mathbf{u}(t) + \eta(\mathbf{I_N}\otimes\mathbf{D})\boldsymbol{\xi}(t)\end{aligned} \tag{2}$$

with the state vector $\mathbf{x} = (\mathbf{x_1}, \ldots, \mathbf{x_N})$ and $\mathbf{x_i} = (x_{i1}, \ldots, x_{id})$. $\otimes$ denotes the Kronecker product. The local node dynamics are $\mathbf{h}(\mathbf{x}) = (\mathbf{h}(\mathbf{x_1}), \ldots, \mathbf{h}(\mathbf{x_N}))$ with $\mathbf{h}(\mathbf{x_i}) = (h_1(\mathbf{x_i}), \ldots, h_d(\mathbf{x_i}))$. The coupling term consists of the $N \times N$-dimensional adjacency matrix $\mathbf{A}$ and the $d \times d$-dimensional local coupling scheme $\mathbf{G}$. The control term consists of the control vector $\mathbf{u} = (\mathbf{u_1}, \ldots, \mathbf{u_N})$ with $\mathbf{u_i} = (u_{i1}, \ldots, u_{id})$, the diagonal $N \times N$ dimensional control matrix $\mathbf{B}$ and the $d \times d$-dimensional local control scheme $\mathbf{K}$. The noise term consists of the noise intensity η and the Kronecker product of an N-dimensional identity matrix $\mathbf{A}$ and the $d \times d$-dimensional local noise scheme $\mathbf{G}$. The stochastic process (Gaussian white noise with variance η) is given by $\boldsymbol{\xi}$. Following boundary conditions are given:

$$\mathbf{x}(t=0) = \mathbf{x_0} \tag{3}$$

The dynamics of an uncoupled FitzHugh-Nagumo oscillator are

$$\mathbf{h}(\mathbf{x}) = \begin{pmatrix}\dot{x}_1\\ \dot{x}_2\end{pmatrix} = \begin{pmatrix}R(x_1) - x_2 + I_{ext}\\ \frac{1}{\tau}(x_1 - \epsilon x_1)\end{pmatrix},$$

with $R(x) = -\alpha x^3 + \beta x^2 - \gamma x$. The parameters are fixed for all following results: $\alpha = 3$, $\beta = 4$, $\gamma = 3/2$, $\tau = 20$, $\epsilon = 0.5$.

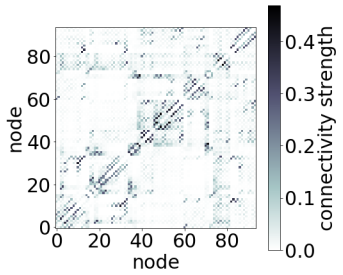

FIG. 1: Weighted adjacency matrix of the network topology. Structural connectivity strength for each pair of $N = 94$ nodes.

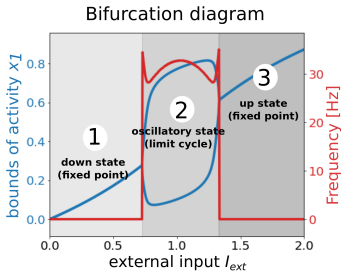

FIG. 2: Bifurcation diagram of an uncoupled FitzHugh-Nagumo node given in equation (**??**).

III. NONLINEAR OPTIMAL CONTROL

A. The cost-functional and its gradient

In this section we consider the manipulation of the introduced network system. This may include controlling the network state as in section (V A) ar the network synchronization as in section (V B). First, we set up a cost-functional and define a control to be optimal, when it is a local minimum of this functional. The network system, as introduced above, is stochastic, but since the control is deterministic the cost-functional F is defined as a mean over noise realizations [1].

$$F(\mathbf{x}(\mathbf{u}), \mathbf{u}) = \langle F_n(\mathbf{x}(\mathbf{u}), \mathbf{u})\rangle = \langle F_n^x(\mathbf{x})\rangle + F^u(\mathbf{u}) \quad (4)$$

where F_n denotes the cost-functional of one noise realization and the angle brackets $\langle\cdot\rangle$ denote the mean over noise realizations. The first term of the cost-functional only implicitly depends on the control and penalizes the deviation to the desired output. When the control task is to switch between bistable states it is defined as the distance of the controlled state to a predefined target state $\mathbf{x}_T(t)$:

$$F_{n,1}^x(\mathbf{x}, t) = \int_0^T \frac{I_p(t)}{2} \|\mathbf{x}(t) - \mathbf{x}_T(t)\|^2_{L^2(0,N)} dt \quad (5)$$

For synchronizing the network dynamics F_n^x is defined as the deviation of the normalized pairwise cross-correlation R_{ij} of the dynamics of each pair of nodes i and j from the target cross-correlation R_T:

$$F_{n,2}^x(\mathbf{x}, t) = \frac{I_p}{4N^2} \sum_{i,j=1}^{N} (R_{ij} - R_T)^2 \quad (6)$$

The second term of the cost-functional penalizes the control signal energy and enforces its directional sparsity in space reducing the number of control sites, as introduced in the work of Casas et al. ([2]):

$$F^u(\mathbf{u}) = \frac{I_e}{2} \int_0^T \|\mathbf{u}(t)\|^2_{L^2(0,N)} dt + I_s \| \Big(\int_0^T \mathbf{u}(t)^2 dt \Big)^{\frac{1}{2}} \|_{L^1(0,N)} \quad (7)$$

With tuning the three variables I_p, I_e and I_s we can alter the weights of the cost-functional's terms. Our goal is to find the optimal control $\overline{\mathbf{u}}$ that minimizes the cost-functional and we pose following minimization problem:

$$\min_{\mathbf{u}} \langle F_n(\mathbf{x}(\mathbf{u}), \mathbf{u})\rangle \quad (8)$$

For its computational solution we apply a conjugate gradient descent method. Since the derivative of the state $\mathbf{x}$ with respect to $\mathbf{u}$ is not defined, the gradient of the cost-functional cannot be derived in a straight-forward way. After applying the Lagrange method we obtain an alternative expression of an N-dimensional time-dependent gradient $\mathbf{g}(t)$ of the cost-functional. This is similar to the result derived by Troeltzsch et al. and Casas et al. ([3–5]).

$$\mathbf{g}(t) = (\mathbf{B} \otimes \mathbf{K})^T \langle \boldsymbol{\phi}(\boldsymbol{x}, \overline{\boldsymbol{u}}, t)\rangle + I_e \overline{\boldsymbol{u}}(t) + I_s \overline{\boldsymbol{\lambda}}(t) \quad (9)$$

and, according to [2],

$$\overline{\lambda_k}(t) = \begin{cases} \frac{\overline{u}_k(t)}{\overline{U}_k} & \text{if } \overline{U}_k \neq 0, \\ -\frac{1}{I_s} \big[(\mathbf{B} \otimes \mathbf{K})^T \langle \boldsymbol{\phi}(\boldsymbol{x}, \overline{\boldsymbol{u}}, t)\rangle\big]_k & \text{otherwise} \end{cases} \quad (10)$$

with $\overline{U}_k = \big(\int_0^T \overline{u}_k(t)^2 dt \big)^{1/2}$ and k in $(1, \ldots, N)$. The system's adjoint state $\boldsymbol{\phi}(\boldsymbol{x}, \overline{\boldsymbol{u}}, t)$ corresponds to the Lagrange multipliers and is defined by a set of linear differential equations:

$$-\dot{\boldsymbol{\phi}}(t) = \big[D_x(\mathbf{h}) + \sigma(\mathbf{A} \otimes \mathbf{G})\big]^T \boldsymbol{\phi}(t) + \nabla_x f_n^x(\boldsymbol{x}, t) \quad (11)$$

where $D_x(\mathbf{h})$ denotes the Jacobian matrix of the state equations of an uncoupled FitzHugh-Nagumo oscillator given in equation (4), $\nabla_x = \big(\frac{\partial}{\partial x_1}, \ldots, \frac{\partial}{\partial x_N}\big)$ and $F_n^x(\boldsymbol{x}) = \int_0^T f_n^x(\boldsymbol{x}) dt$ The adjoint state has a boundary condition at final time $\boldsymbol{\phi}(T) = \mathbf{0}$ and must therefore be solved backwards in time. See Supplemental Material at [URL will be inserted by publisher] for a detailed derivation of the equations (9) and (11).

B. Numerical solution of the minimization problem

A conjugate gradient method is applied to numerically solve the minimization problem given in equation (8). We calculate the the network state and adjoint state given in equations (2) and (9) with the fourth order Runge-Kutta method. The direction for each step of the conjugate gradient algorithm is defined with the Polak Ribiere method, while its stepsize is derived using simple bisection. In the following the iteration steps of the applied Fletcher and Reeves method are presented in detail.

We initialize at iteration $i = 0$ with defining an initial control $\boldsymbol{u_0}$ and setting 20 noise realizations. The corresponding states $\boldsymbol{x}_0(t)$ and the adjoint states $\boldsymbol{\phi}_0(t)$ given in equations (**??**) and (11) are calculated for every noise realization. The associated cost-functional's time dependent gradient $\boldsymbol{g}(t)$ given in equation (9) is evaluated. The descent direction is initialized with $\boldsymbol{d}_0(t) = -\boldsymbol{g}(t)$.

while $\|\boldsymbol{g}(t)\|_\infty > 10^{-5}$:

1. compute the stepsize s_k using bisection
2. set $\boldsymbol{u}_{k+1}(t) = \boldsymbol{u}_k(t) + s_k \boldsymbol{d}_k(t)$
3. calculate the states $\boldsymbol{x}_{k+1}(t)$ and the adjoint states $\boldsymbol{\phi}_{k+1}(t)$ for every noise realization, as well as the mean adjoint state over all noise realizations $\langle \boldsymbol{\phi}_{k+1}(t) \rangle$.
4. evaluate the gradient $\boldsymbol{g}_{k+1}(t)$
5. compute β_k using the Polak-Ribiere method: $\beta_k = \frac{\boldsymbol{g}_{i+1}(\boldsymbol{g}_{i+1} - \boldsymbol{g}_i)}{\|\boldsymbol{g}_{i+1}\|^2}$
6. set the direction $\boldsymbol{d}_{k+1}(t) = -\boldsymbol{g}_{k+1}(t) + \beta_k \boldsymbol{d}_k(t)$
7. if $\boldsymbol{d}_{k+1}(t)$ is not a descent direction set $\boldsymbol{d}_{k+1}(t) = -\boldsymbol{g}_{k+1}(t) \rangle$
8. set $k = k + 1$

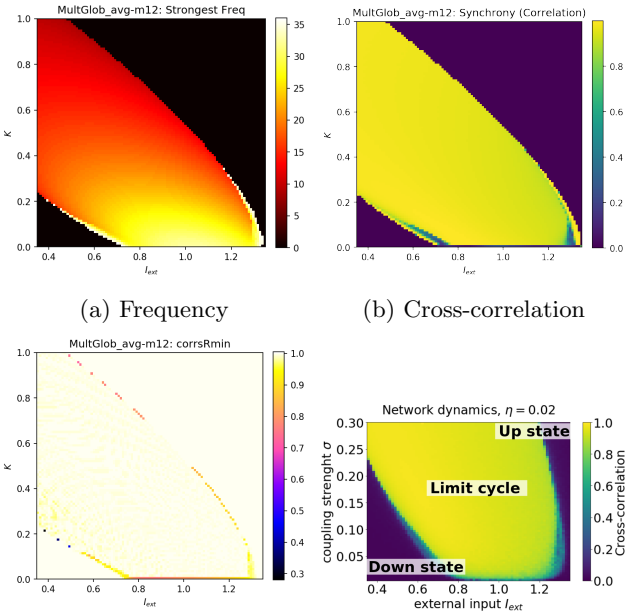

(a) Frequency (b) Cross-correlation

(c) Multistability (d) Cross-corr. with noise

FIG. 3: Different properties of the dynamic landscape that define the state space of the network.

IV. STATE SPACE EXPLORATION

Before any control can be applied to the network, it is crucial to have a through understanding of the dynamic properties of the network. In the upcoming examples we will switch between dynamical states of the network, here we first define what a network state is in the first place and then explore the behavior of the system for different parameter configurations and initialization. For simplicity, we characterize a state by three main properties: 1.) Synchrony, measured by the correlation between the time traces of all nodes. 2.) Frequency, represented by the frequency with the highest spectral power among all nodes. 3.) Multistability, which is detected by correlating timetraces with the same parameter configuration but different initial conditions. Other measures that are frequently used in neuroscience like the metastability or ... are omitted here since they are not directly relevant for the control.

In figure **??**, every pixel shows the synchrony of the 94 network nodes, measured by their cross-correlation:

$$c = \int_{t_0}^{t_0+T} \mathrm{d}t \frac{(\mathbf{x} - \mathrm{mean}(\mathbf{x}))^2}{\mathrm{std}(\mathbf{x})} \tag{12}$$

In the non-oscillatory states, where all nodes are either settled at the lower or upper limit cycle (cf. dynamics of a single node in figure 2), c is not defined since $\mathrm{std}(\mathbf{x}) \to 0$ but are still set to zero for illustration purposes. Panels **??** and **??** show the sharp transition between the two fixed points (down and up state) and the oscillatory state, where either the external input I_{ext} or

the network coupling scaled with strength σ drove some or all nodes in the limit cycle. For $\sigma = 0$, all nodes behave independently and the data is equivalent to the bifurcation diagram of a single node (figure 2). We observe the high frequency of $35Hz$ along the bifurcation line with low coupling strength in figure **??**, characteristic for a single node close to either bifurcation. With increasing coupling strength, the timescale of the oscillation is increasingly dominated by network effects Adding noise to the dynamics, as seen in figure **??**, does not change the overall dynamics for most parameter configurations. At the bifurcation line, however, noise drives a network for limited time periods from a fixed point into oscillation. While most parts of the state space no or show synchronous oscillation, in the parameter regions close to the bifurcation with $I_{ext} \gg]sigma \sum_{i=1}^{N} A_{ki} x_{[}1i]$, so the input from the other node is much smaller than the external input, the dynamics of the individual nodes are more independent and therefore less synchronous. In section V B we apply the optimal control formalism to increase the synchrony in such a network.

The other application, demonstrated in this study (section V A), is to find the optimal control to switch from one stable state to another. Hence, we search for multistability in the network by simulating the system for the same parameter configurations with multiple initial conditions. The resulting activity traces of all nodes $x_1'(t)$ and $x_1''(t)$ are then correlated over a timescale longer than their oscillation periods to be agnostic about their phase. If the correlation of one initialization to another one is different from its autocorrelation, this indicates that there is not only one stable solution (see figure 4 for an example).

state switching due to noise, show example, is a know phenomenon in coupled oscillators (cite physics paper micha) and was related to neural activity by micha.

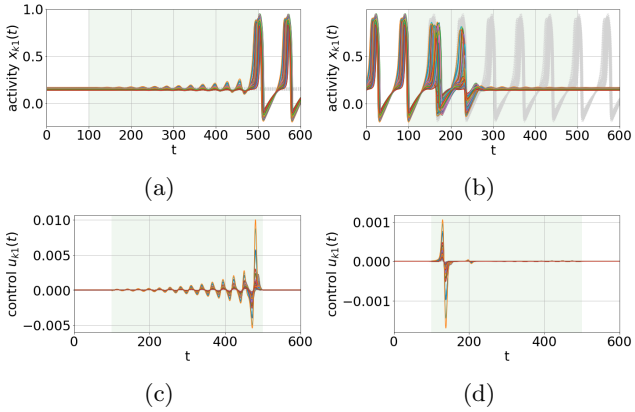

FIG. 4: Examples of state switching with optimal control close to the low bifurcation line. (a,b): Activity of each node over time. The colored lines show the controlled scenario, the gray lines show the uncontrolled scenario. (c,d) Corresponding optimal control input to each node. The green shaded area indicates the control time. Parameters: $\mu = 0.378$ and $\sigma = 0.21$ (point A in figure (3)), $\eta = 0.0$, $I_p^* = 0.0005$, $I_e = 1.0$, $I_s = 0$.

V. APPLICATIONS

A. Switching between bistable network states

Close to the bifurcation lines of the noise-free network dynamics we observe bistable states. In this section we present optimal control inputs that induce a switch between the stable states we conclude that the driver nodes leading this transition differ depending on which of the bifurcation lines we are close to. Furthermore, we discuss the frequency and phase of the control input.

For this application we minimize the cost functional given in equation (4). We insert equation (5) to penalize the deviation from the target state and equation (7) to penalize the energy cost of the control and enforce its sparsity in space. We penalize the deviation from the target state only in the last 25 time units of the control time giving the system time to transition from one state to the other. For this we set the parameter in equation (5) $I_p(t) = I_p^*$ for $t > T - 25$ and $I_p = 0$ else. We choose the low state as the initial state and the high state as the target state and vice versa. The optimal control was calculated for all phase shifts between the initial and the target state and for the results shown here the phase relationships resulting in the lowest minimum of the functional is shown.

We first set the parameter in equation (7) $I_s = 0$ and thus do not demand the control to be sparse. In figures (4) and (5) the switching network dynamics and the corresponding optimal controls are shown for parameters chosen to be clos eto the low and the high bifurcation line, respectively. We note that both attractors are stable and the system stays in the target state even when the control is turned off. When switching from the low to the high state in figures (4 a,c) and (5 a,c) resonance effects are applied and the frequency of he control is determined by the frequency of the target state. In case the low state is a fixed point, as seen in figure (4 a,c), the frequency corresponds to the frequency of the fixed point's focus. When switching from the high to the low state in figures (4 b,d) and (5 b,d) the optimal control ?..

With increasing the parameter I_s of the cost functional we can tune the number of controlled nodes. The control energy at each control site depending on the sparsity parameter is shown in figure (13). The results show that at the low bifurcation line nodes with a high weighted degree, so called hubs, act as driver nodes inducing the attractor switching. On the contrary, at the high bifurcation line nodes with low and intermediate weighted degrees play a prominent role. This result shows that the node sensitivity/susceptibility? to an external input plays an important role in choosing the control sites in an

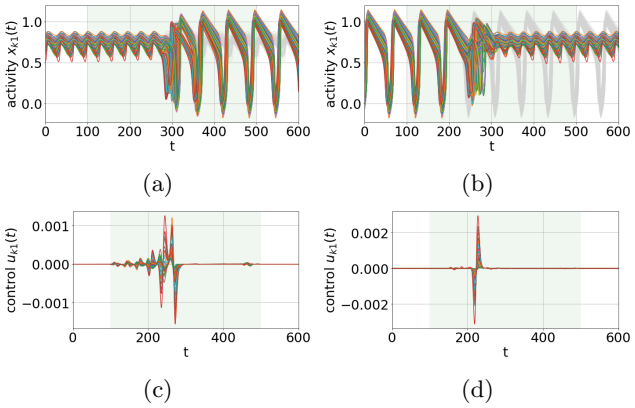

FIG. 5: Examples of state switching with optimal control close to the high bifurcation line. (a,b): Activity of each node over time. The colored lines show the controlled scenario, the gray lines show the uncontrolled scenario. (c,d) Corresponding optimal control input to each node. The green shaded area indicates the control time. Parameters: $\mu = 1.22$ and $\sigma = 0.26$ (point B in figure (3)), $\eta = 0.0$, $I_p^* = 7 \cdot 10^{-5}$, $I_e = 1.0$, $I_s = 0$.

optimal control scenario. Furthermore, when decreasing the number of control sites, we need to compensate with a higher control energy.

B. Synchronizing the network dynamics

In this section we show applications of optimal control inputs that synchronize the network dynamics. We discuss the control mechanisms and its dependence on the noise strength. Furthermore, we show that fully synchronizing the dynamics with a low number of control sites is not possible.

Figures (7) and (8) show examples of the controlled (synchronous) and uncontrolled (asynchronous) time-traces and the corresponding control input. Since the synchronous state is not a stable solution of the uncontrolled system, it does not last when the control is switched off. For a system without noise shown in figures (7 a,c) and (8 a,c) the asynchronous behaviour arises due to the different frequencies of nodes with varying coupling inputs. The control balances out the differences acting mainly on the high and the low degree nodes, not the intermediate ones, see figure (8). In the case of a noisy system shown in figures (7 b,d) and (8 b,d) the control drives the oscillations. As can be seen in figure (8) the low degree nodes get the highest input, since they are less connected to the network and therefore more likely to exhibit deviating behaviour.

In figure (11) the relation of the network cross-correlation to the sparsity parameter I_s is shown. Fully synchronizing the network with sparse control is not pos-

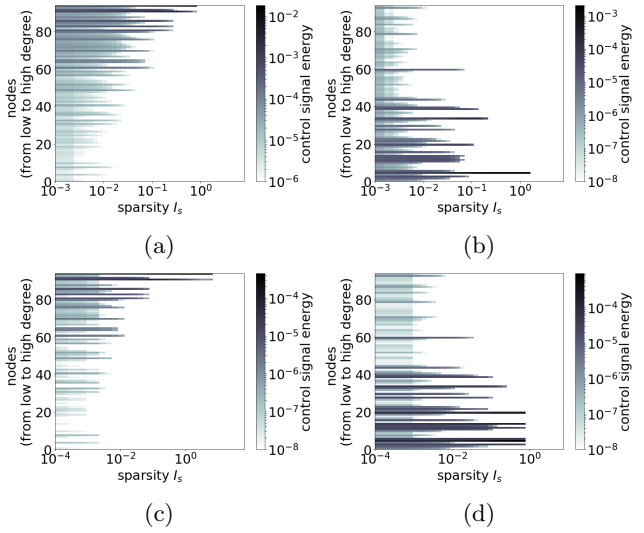

FIG. 6: State switching with sparse optimal control. The nodes sorted from lowest to highest degree over the parameter of the cost functional I_s weighing the sparsity of the control. The color code denotes the optimal control energy input on each node. (a,c) Parameters close to the low bifurcation line as in figure (4). (b,d) Parameters close to the high bifurcation line as in figure (5). (a,b) Switching from the low to the high state. (c,d) Switching from the high to the low state.

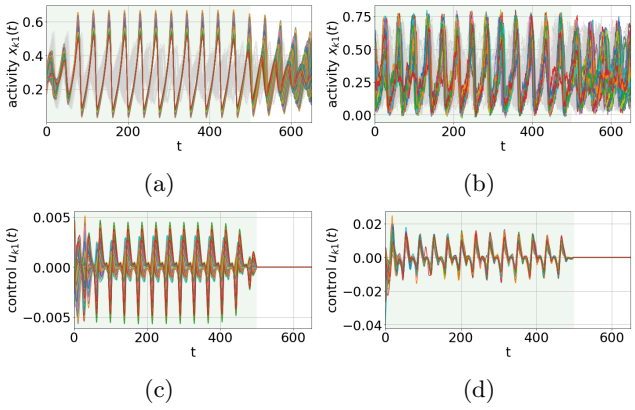

FIG. 7: Examples of state switching with optimal control close to the low bifurcation line. (a,b) Activity of each node over time. The colored lines show the controlled scenario, the gray lines show the uncontrolled scenario. (c,d) Corresponding optimal control input to each node. The green shaded area indicates the control time. (a,c) noise-free dynamics, $\eta = 0.0$. (b,d) noisy dynamics, $\eta = 0.024$. Parameters: $\mu = 0.7$ and $\sigma = 0.025$ (point C in figure (3)), $I_p = 0.1$, $I_e = 1.0$, $I_s = 0$.

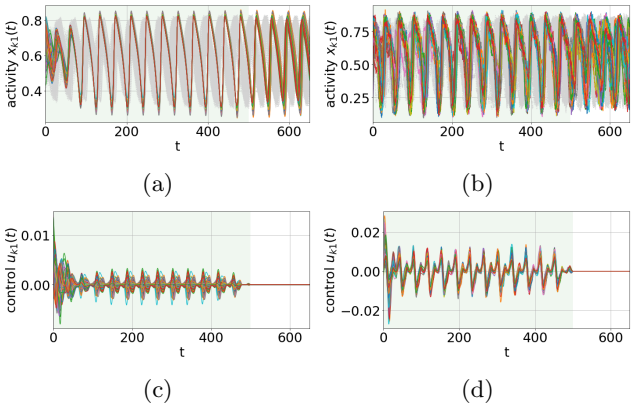

FIG. 8: Examples of state switching with optimal control close to the high bifurcation line. (a,b) Activity of each node over time. The colored lines show the controlled scenario, the gray lines show the uncontrolled scenario. (c,d) Corresponding optimal control input to each node. The green shaded area indicates the control time. (a,c) noise-free dynamics, $\eta = 0.0$. (b,d) noisy dynamics, $\eta = 0.024$. Parameters: $\mu = 1.3$ and $\sigma = 0.025$ (point D in figure (3)), $I_p = 0.1$, $I_e = 1.0$, $I_s = 0$.

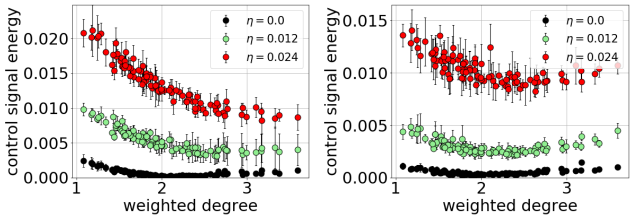

FIG. 9: Mean correlation of the optimal control input to the weighted node degree for different noise levels. The error bars show the standard deviation over 10 realizations. (a) Parameters: $\mu = 0.7$ and $\sigma = 0.025$ close to the low bifurcation line (point C in figure (3)). (b) Parameters: $\mu = 1.3$ and $\sigma = 0.025$ close to the high bifurcation line (point D in figure (3)). Other parameters: $I_p = 0.1$, $I_e = 1.0$, $I_s = 0$.

sible. Synchronization seems to be a collective behaviour, and unlike state switching shown in the section above, can not be succeeded with using only a few control sites.

VI. LINEAR VS. NONLINEAR CONTROL

[6] [7] [8] [9]

[1] Wilhelm Stannat and Lukas Wessels. Deterministic control of stochastic reaction-diffusion equations, 2019.

[2] Eduardo Casas, Roland Herzog, and Gerd Wachsmuth. Analysis of spatio-temporally sparse optimal control problems of semilinear parabolic equations. *ESAIM: Control, Optimisation and Calculus of Variations*, 23(1):263–295, 2017.

[3] Eduardo Casas, Christopher Ryll, and Fredi Tröltzsch. Sparse optimal control of the schlögl and fitzhugh-nagumo systems. *Comput. Methods Appl. Math*, 1:1–29, 2001.

[4] Fredi Tröltzsch. *Optimal control of partial differential equations: theory, methods, and applications*, volume 112. American Mathematical Soc., 2010.

[5] Rico Buchholz, Harald Engel, Eileen Kammann, and Fredi Tröltzsch. On the optimal control of the schlögl-model. *Computational Optimization and Applications*, 56(1):153–185, 2013.

[6] Sarah Feldt Muldoon, Fabio Pasqualetti, Shi Gu, Matthew Cieslak, Scott T Grafton, Jean M Vettel, and Danielle S Bassett. Stimulation-based control of dynamic brain networks. *PLoS computational biology*, 12(9), 2016.

[7] CJ Honey, O Sporns, Leila Cammoun, Xavier Gigandet, Jean-Philippe Thiran, Reto Meuli, and Patric Hagmann. Predicting human resting-state functional connec-

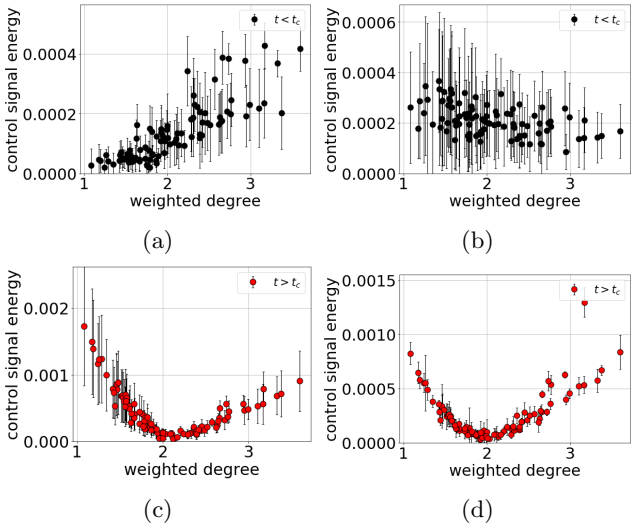

FIG. 10: Mean correlation of the optimal control input to the weighted node degree for the noise-free case. The error bars show the standard deviation over 10 realizations. (a,b) The control signal from time $t = 0$ until time $t = t_c$ is considered. (c,d) The control signal from time $t = t_c$ until time $t = T$ is considered. (a,c) Parameters: $\mu = 0.7$ and $\sigma = 0.025$ close to the low bifurcation line (point C in figure (3)). (b,d) Parameters: $\mu = 1.3$ and $\sigma = 0.025$ close to the high bifurcation line (point D in figure (3)). Other parameters: $I_p = 0.1$, $I_e = 1.0$, $I_s = 0$.

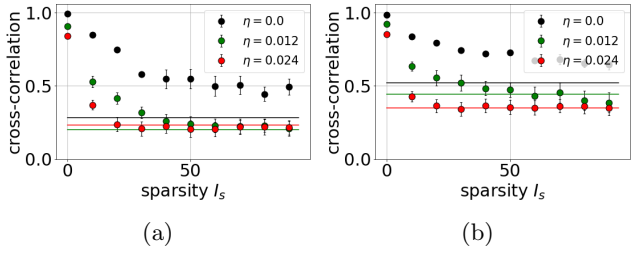

FIG. 11: Synchronization with sparse optimal control for different noise levels. Network cross correlation over the parameter of the cost functional I_s weighing the sparsity of the control. The mean and standard deviation over 5!? realizations of the optimization and the evaluation of ? noise realizations. bars are the(a) Parameters: $\mu = 0.7$ and $\sigma = 0.025$ close to the low bifurcation line (point C in figure (3)). (b) Parameters: $\mu = 1.3$ and $\sigma = 0.025$ close to the high bifurcation line (point D in figure (3)). Other parameters: $I_p = 0.1$, $I_e = 1.0$, $I_s = 0$.

tivity from structural connectivity. *Proceedings of the National Academy of Sciences*, 106(6):2035–2040, 2009.

[8] Roberto F Galán. On how network architecture determines the dominant patterns of spontaneous neural activity. *PloS one*, 3(5), 2008.

[9] Shi Gu, Fabio Pasqualetti, Matthew Cieslak, Qawi K

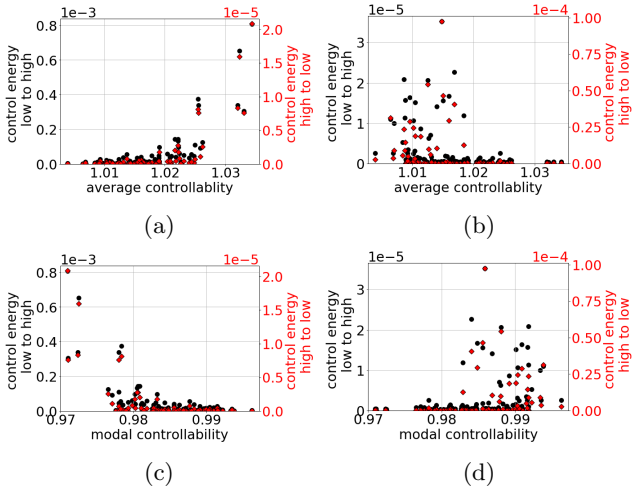

FIG. 12: State switching with sparse optimal control. The nodes sorted from lowest to highest degree over the parameter of the cost functional I_s weighing the sparsity of the control. The color code denotes the optimal control energy input on each node. (a,b) Parameters close to the low bifurcation line as in figure (4). (c,d) Parameters close to the high bifurcation line as in figure (5). (a,c) Switching from the low to the high state. (b.d) Switching from the high to the low state.

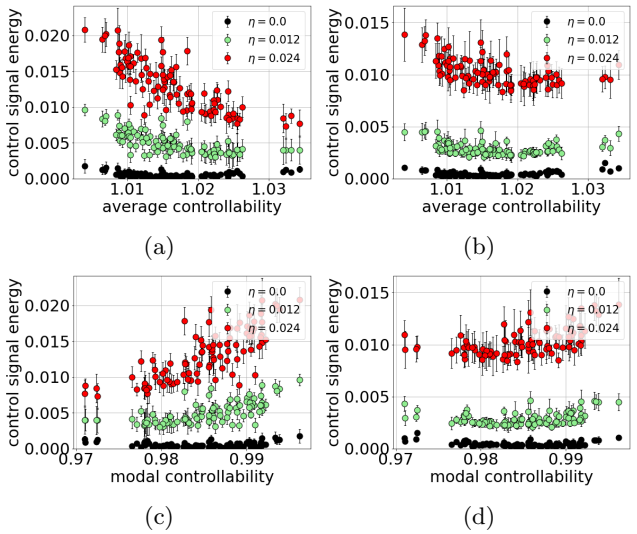

FIG. 13: State switching with sparse optimal control. The nodes sorted from lowest to highest degree over the parameter of the cost functional I_s weighing the sparsity of the control. The color code denotes the optimal control energy input on each node. (a,b) Parameters close to the low bifurcation line as in figure (4). (c,d) Parameters close to the high bifurcation line as in figure (5). (a,c) Switching from the low to the high state. (b.d) Switching from the high to the low state.

Telesford, B Yu Alfred, Ari E Kahn, John D Medaglia, Jean M Vettel, Michael B Miller, Scott T Grafton, et al. Controllability of structural brain networks. *Nature communications*, 6(1):1–10, 2015.

VII. MISSING

- Mathematical proof of the derivation of the cost functional's gradient. (Prof. Stannat)
- Error in code.
- Too few runs for calculating the mean and std in the synchronization section
- In the case of synchronizing the dynamics the resulting optimal control might just be an local optimum
- In figure 10 the controlled cross correlation can be worse than the uncontrolled. More noise realizations should be taken for the calculation of the optimal control. (for the results plotted 20 noise realizations where used)
- Small noise can be added for the state switching application